

# Late time evolution of unforced inviscid two-dimensional turbulence

DAVID G. DRITSCHEL<sup>1</sup>†, RICHARD K. SCOTT<sup>1</sup>,  
CHARLIE MACASKILL<sup>2</sup>, GEORG A. GOTTWALD<sup>2</sup>  
AND CHUONG V. TRAN<sup>1</sup>

<sup>1</sup>School of Mathematics and Statistics, University of St Andrews, St Andrews KY16 9SS, UK

<sup>2</sup>School of Mathematics and Statistics, University of Sydney, NSW 2006, Australia

(Received 15 November 2008; revised 9 July 2009; accepted 9 July 2009; first published online 19 October 2009)

We propose a new unified model for the small, intermediate and large-scale evolution of freely decaying two-dimensional turbulence in the inviscid limit. The new model's centerpiece is a recent theory of vortex self-similarity (Dritschel *et al.*, *Phys. Rev. Lett.*, vol. 101, 2008, no. 094501), applicable to the intermediate range of scales spanned by an expanding population of vortices. This range is predicted to have a steep  $k^{-5}$  energy spectrum. At small scales, this gives way to Batchelor's (Batchelor, *Phys. Fluids*, vol. 12, 1969, p. 233)  $k^{-3}$  energy spectrum, corresponding to the (forward) enstrophy (mean square vorticity) cascade or, physically, to thinning filamentary debris produced by vortex collisions. This small-scale range carries with it nearly all of the enstrophy but negligible energy. At large scales, the slow growth of the maximum vortex size ( $\sim t^{1/6}$  in radius) implies a correspondingly slow inverse energy cascade. We argue that this exceedingly slow growth allows the large scales to approach equipartition (Kraichnan, *Phys. Fluids*, vol. 10, 1967, p. 1417; Fox & Orszag, *Phys. Fluids*, vol. 12, 1973, p. 169), ultimately leading to a  $k^1$  energy spectrum there. Put together, our proposed model has an energy spectrum  $\mathcal{E}(k, t) \propto t^{1/3}k^1$  at large scales, together with  $\mathcal{E}(k, t) \propto t^{-2/3}k^{-5}$  over the vortex population, and finally  $\mathcal{E}(k, t) \propto t^{-1}k^{-3}$  over an exponentially widening small-scale range dominated by incoherent filamentary debris.

Support for our model is provided in two parts. First, we address the evolution of large and ultra-large scales (much greater than any vortex) using a novel high-resolution vortex-in-cell simulation. This verifies equipartition, but more importantly allows us to better understand the approach to equipartition. Second, we address the intermediate and small scales by an ensemble of especially high-resolution direct numerical simulations.

---

## 1. Introduction

One of the most fascinating aspects of fluid flows is turbulence. Turbulence is inherently nonlinear, operating over a wide range of spatial and temporal scales (cf. Tabeling 2002; Davidson 2004; Lesieur 2008 and the references therein). This range grows with the Reynolds number, or the inverse of viscosity. Yet turbulence is not a state of complete disorder, but rather a semi-organized state exhibiting coherent structures (e.g. vortices) and self-similar scaling properties (e.g. power-law spectra).

† Email address for correspondence: dgd@mcs.st-and.ac.uk

Turbulence is found in a great number of physical systems, ranging in scale from quantum to astrophysical dimensions. There is little hope of a universal theory applicable to all systems, but some idealized systems now appear to be within reach. The simplest, and the most widely studied, is governed by the two-dimensional Navier–Stokes equations, or Euler equations in the inviscid unforced situation considered here. This system evolves purely by advection of a (scalar) vorticity, which moreover is conserved on fluid particles. The system exhibits a dual cascade of energy (to large scales) and enstrophy (to small scales), but conserves total energy and enstrophy (Kraichnan 1967; Batchelor 1969).

Much of the research on ‘freely-decaying’ two-dimensional turbulence has focused on small to intermediate scales, the so-called ‘inertial range’ lying between the most energetic scale and (if present) the dissipative scale. Over this range, Batchelor (1969) used dimensional arguments to predict a  $k^{-3}$  form of the energy spectrum (where  $k$  is the wavenumber), which has since been nearly universally found in numerical simulations (see Davidson 2004 and references therein).

It has been recognized for some time that the  $k^{-3}$  decay of the energy spectrum, found independently by Kraichnan (1967) and Batchelor (1969) in two-dimensional turbulence, is not sufficient to explain the observed steeper spectra (see for example McWilliams 1984). These theories are local in wave number space and do not take into account the nonlocal effect of vortices in transporting energy and enstrophy. Since then, several scaling theories have been proposed stressing the importance of vortices for the energy transport in spectral space. Benzi, Patarnello & Santangelo 1988 and Benzi *et al.* (1992) linked the statistics of vortex populations to the energy spectrum. They numerically fitted an algebraically decaying vortex population with number density  $n(A, t) \sim A^{-\xi}$  (where  $n(A, t)dA$  gives the average number of vortices with areas between  $A$  and  $A + dA$  over a sample area  $A_s$  in the plane) to deduce that the energy spectrum associated with the vortices decays more steeply than predicted by the Batchelor scaling (Batchelor 1969).

The temporal scaling of the vortex number density was addressed in Carnevale *et al.* (1991) and Weiss & McWilliams (1993). Carnevale *et al.* (1991) assumed that, in addition to energy, the maximal vorticity during vortex interactions is conserved. Dimensional arguments then lead to an algebraic decay in time of the vortex number density  $n(A, t)$ . Their analysis however assumes vortices of one particular size, and does not predict the value of the scaling exponent.

In Dritschel *et al.* (2008) we presented a model which unifies these spatial and temporal scaling theories. We argued that, as a result of repeated vortex collisions, a self-similar vortex population naturally arises in two-dimensional turbulence, and that this population is characterized by a vortex number density  $n(A, t) \propto t^{-2/3} A^{-1}$ . This decay occurs principally through collisions involving a ballistic dipole and a monopole (cf. Dritschel & Zabusky 1996). Sire & Chavanis (2000) and Laval *et al.* (2001), on the other hand, argued that three body collisions lead to a faster  $t^{-1}$  decay of  $n(A, t)$  at late times when the distribution of vortices becomes very dilute, but they did not consider a distribution of vortex sizes. Sopik, Sire & Chavanis (2009, personal communication) have since independently derived a  $t^{-2/3}$  decay for shorter times based on different arguments.) It is difficult, however, to conceive of another timescale apart from the inverse of the r.m.s. vorticity  $\omega_{rms}$ ; hence there should be no distinction between ‘late’ and ‘shorter’ times if both greatly exceed  $\omega_{rms}^{-1}$ . We argue that the  $t^{-2/3}$  decay of the vortex number density, derived in Dritschel *et al.* (2008), persists for *all* time in an infinite domain and in the absence of viscosity.

The self-similar form  $n(A, t) \propto t^{-2/3} A^{-1}$ , following Benzi *et al.* (1988), implies an energy spectrum  $\mathcal{E}(k, t) \propto t^{-2/3} k^{-5}$  over the range of scales containing the vortex population. Moreover, this implies that the enstrophy in the vortex population decays like  $t^{-1/3}$  through vortex collisions, which produce incoherent filamentary debris carrying nearly all of the enstrophy to small scales at late times. Meanwhile, for consistency, the mean radius of the largest vortices – proportional to  $\ell = \sqrt{E/Q}$  where  $E$  and  $Q$  are the total (vortex) energy and enstrophy – slowly grows like  $t^{1/6}$ , sending energy to progressively larger scales at a diminishing rate proportional to  $t^{-5/6}$ .

These predictions were verified by an ensemble of ultra-high resolution numerical simulations, and are consistent with previous numerical simulations (Benzi *et al.* 1992; Weiss & McWilliams 1993; Clercx, Maassen & van Heijst 1999; Bracco *et al.* 2000). The  $t^{1/6}$  growth of the integral scale  $\ell$  is much slower than the  $t^1$  growth predicted by Batchelor (1969), and is significantly slower than the  $t^{1/2}$  growth argued by Lowe & Davidson (2005), building on the phenomenological scaling theory of Bartello & Warn (1996). Their  $t^{1/2}$  growth, however, was only demonstrated at relatively low Reynolds number.

The present paper addresses the spatial and temporal scaling behaviour at large scales, and connects it with that of the vortex population and filaments at intermediate and small scales, addressed in Dritschel *et al.* (2008). There has been surprisingly little research done on the large-scale structure of two-dimensional turbulence. Exceptions include Chasnov (1997), Ossai & Lesieur (2001), Lowe & Davidson (2005) and Davidson (2007). Here, we consider scales larger than any vortex, and moreover in an *infinite* domain in order to examine the limit  $t \rightarrow \infty$  without the effects of domain boundaries or periodicity. Thereby, the flow can never reach statistical equilibrium and must continue evolving forever. We argue that as the flow evolution slows down at late times, the large-scale evolution approaches *equipartition*, in which a linear combination of energy and enstrophy becomes uniformly distributed among Fourier modes (Kraichnan 1967; Orszag 1970; Fox & Orszag 1973 and many others; see Lesieur 2008, ch. 10 and references therein). In time, equipartition spreads to increasingly large scales where the energy alone is approximately uniform among Fourier modes, implying a  $k^1$  energy spectrum there. This is illustrated in §2 through a novel point-vortex experiment starting from small-scale initial conditions. In §3, vortex self-similarity (Dritschel *et al.* 2008) and large-scale equipartition are combined in a model of the long-time turbulent decay. Using only conservation of energy and enstrophy, and assuming that the smallest scales stretch exponentially fast (at a constant growth rate), this model predicts that the steep  $k^{-5}$  energy spectrum associated with the vortex population slowly spreads over the range  $m(t) \lesssim k \lesssim f(t)$ , with  $f(t) \sim t^{1/6}$  and  $m(t) \sim t^{-1/6}$ . Meanwhile, the shallower  $k^{-3}$  energy spectrum associated with incoherent filamentary debris is pushed out to ever higher wavenumbers,  $k \gtrsim f(t) \sim t^{1/6}$ . Support for this model is provided in §4 via a large ensemble of high-resolution numerical simulations. The paper concludes in §5.

## 2. Large-scale dynamics

At scales much larger than any vortex, vortices appear point-like yet may collectively exhibit large-scale motions, e.g. in the form of clusters of like-signed vortices. This *self-organization* was discussed early on in this context by Onsager (1949) and many others since (cf. Eyink & Sreenivasan 2006 and references therein). Onsager used a thermodynamical analogy to predict clustering depending on properties of the

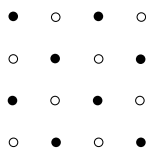


FIGURE 1. Staggered array of point vortices (● = positive, ○ = negative) in a single grid box used as the initial conditions. The vortices are separated by  $\Delta x/4$  both horizontally and vertically, where  $\Delta x$  is the grid size.

initial vortex distribution, like the proximity of like or opposite-signed vortices (for further developments, see Joyce & Montgomery 1973; Montgomery & Joyce 1974; Miller 1990; Robert 1991; Robert & Sommeria 1991; Eyink & Spohn 1993, for example).

Onsager considered point vortices having finite circulations but infinitesimal size, and it seems appropriate to revisit this model to understand the development of large-scale order in turbulence. Specifically, we wish to understand the form of the energy spectrum developing from an inverse cascade of energy from an initial small-scale reservoir containing disorganized or incoherent vortical motions.

To this end, we carried out a large simulation of  $4096^2 \approx 17$  million vortices in a two-dimensional doubly-periodic domain. We used the vortex-in-cell (VIC) method (cf. Christiansen & Zabusky 1973) on a  $1024^2$  grid to speed up the calculation. In the VIC method, the vorticity at a grid point is obtained by a weighted sum of the vortex circulations in the surrounding 4 grid boxes, using the standard Fresnel weights associated with bi-linear interpolation. The gridded vorticity field  $\omega$  so obtained is then ‘inverted’ via fast Fourier transforms (FFTs) to obtain the streamfunction  $\psi = \Delta^{-1}\omega$  and the velocity field  $\mathbf{u} = \nabla^\perp \psi = (-\psi_y, \psi_x)$  on the grid. Finally,  $\mathbf{u}$  is interpolated (bi-linearly) to the positions of the 17 million vortices and used to advect them forward within a fourth-order Runge–Kutta time-stepping scheme.

So far this is standard. The novelty, we believe, lies in our set up of the initial conditions. To track the inverse energy cascade, we had to ensure that initially very little energy was contained in scales larger than the grid size. This is virtually impossible to achieve from a random distribution of vortices, even 17 million of them. Random placement invariably leads to a  $k^{-1}$  energy spectrum (as discussed by Davidson 2007), spoiling any hope of observing an inverse cascade. Instead, in each of the  $1024^2$  grid boxes, we placed 16 vortices in a nearly regular array with 8 positive vortices (each with circulation  $\Gamma$ ) and 8 negative vortices (each with circulation  $-\Gamma$ ), staggered as shown in figure 1. For a perfectly regular array in each grid box, the average vorticity contributed by all 64 vortices in the 4 grid boxes surrounding each grid point is identically zero, so there is in fact no energy (or enstrophy) at and above the grid scale.

To get things going, each vortex is displaced in  $x$  and in  $y$  by a uniformly-distributed random number lying between  $-0.001\Delta x$  and  $+0.001\Delta x$  where  $\Delta x$  is the grid spacing. This generates a weak  $k^1$  energy spectrum which is subsequently overwhelmed by the inverse cascade (see figure 2 and discussion below).

The vortex circulation  $\Gamma$  is chosen so that the vorticity  $\omega$  would be  $4\pi$  for a regular array of positive vortices in the grid boxes surrounding a given grid point. This requires  $16\Gamma = 4\pi(\Delta x)^2$ . The vorticity-based time scale is then unity.

We now turn to the results of this simulation. By time  $t = 100$ , there is already a huge growth of energy at large scales, and the energy continues to grow (as energy cascades from subgrid to supergrid scales) until about  $t = 500$ . Figure 2 shows the

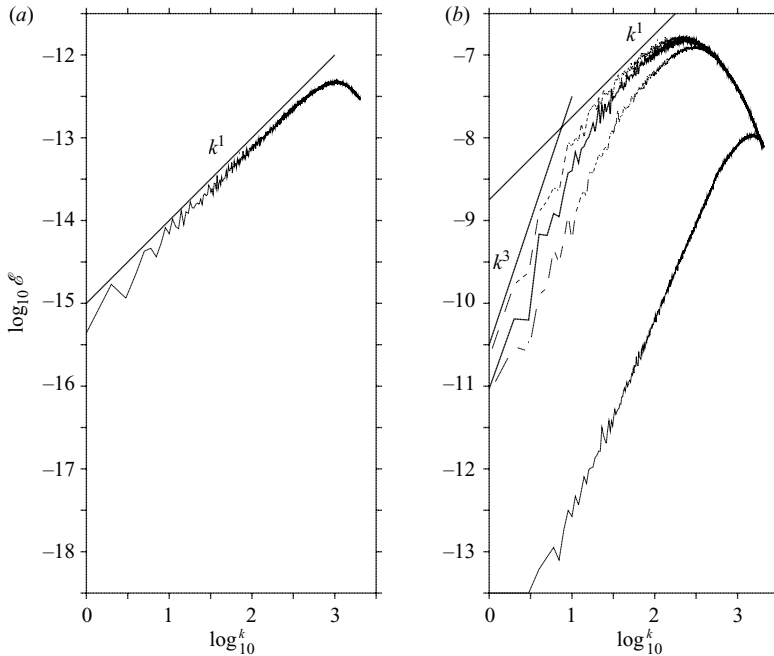


FIGURE 2. (a) Energy spectra at  $t=0$  and (b) at times  $t=100$  (thin solid line), 200 (long dashed line), 300 (bold solid line) and 400 (short dashed line).

energy spectra  $\mathcal{E}(k, t)$  at  $t=0$  (figure 2a), and  $t=100, 200, 300$  and  $400$  (figure 2b). Note there is a difference of 5 orders of magnitude in the energy ranges plotted in the two plots. From  $t=500$  onwards, the energy evolves much more slowly, and fastest at the largest scales (or lowest wavenumbers) — see figure 3(a) for  $t=500, 1000, 1500$  and  $2000$ , and figure 3(b) for  $t=2000$  individually. Figure 4 shows the temporal evolution of the total energy and enstrophy. One sees clearly the initial rapid increase in energy and enstrophy and the slower evolution to a plateau at later times.

The most striking feature exhibited by the energy spectra in figure 3 is their convergence to some fixed form over an increasingly wide range of wavenumbers. In time, the growth in energy becomes confined to progressively lower wavenumbers or larger scales, as can be seen in the streamfunction field  $\psi$ , shown in figure 5 at  $t=200, 500$  and  $2000$ . The largest scale in  $\psi$  coincides with the transition from  $\mathcal{E} \sim k^1$  to  $k^3$ .

A  $k^3$  range is expected, for sufficiently small  $k$ , based on the mathematical analysis of Tran & Dritschel (2006), who proved that  $\mathcal{E}(k, t) \leq Ck^3t^2$ , for some constant  $C$  proportional to the square of the total energy, starting from  $\mathcal{E}(k, 0)=0$  over this wavenumber range. Davidson (2007) showed that the  $k^3$  energy spectrum can be related to the non-vanishing total angular momentum of the vortices through the Loitsyansky integral. Chasnov (1997), Ossai & Lesieur (2001) and Lowe & Davidson (2005) also found the low-wavenumber  $k^3$  scaling (so long as periodicity is insignificant), though Ossai & Lesieur (2001) suggest  $\mathcal{E}(k, t) \propto k^3t^{2.5}$  (in turn much slower than the  $t^4$  growth predicted by Batchelor 1969).

The growth in  $\mathcal{E}(k, t)$  at small  $k$  is not incompatible with the widening  $k^1$  range seen in figure 3 (and quantified below), and, for example, could be modelled by the

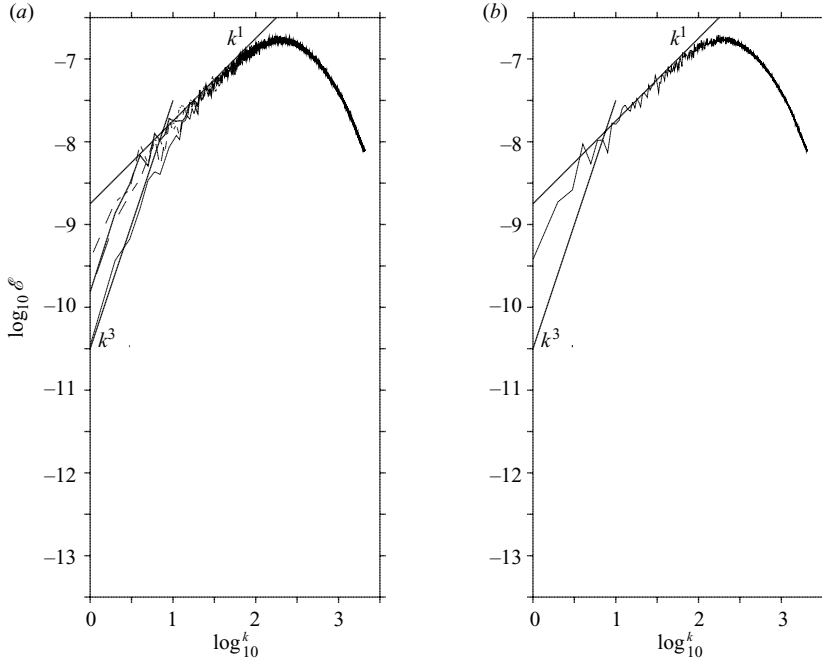


FIGURE 3. Energy spectra (a) at times  $t = 500$  (thin solid line), 1000 (long dashed line), 1500 (bold solid line) and 2000 (short dashed line), and (b) at  $t = 2000$  individually.

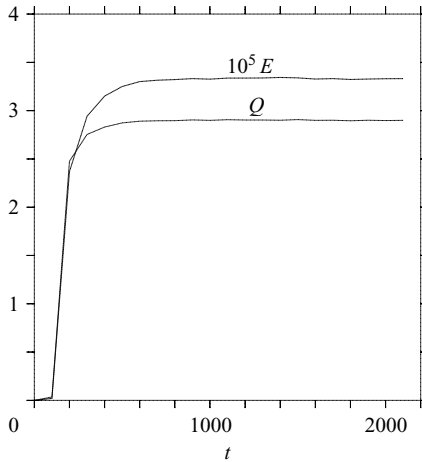


FIGURE 4. Total energy  $E$  (multiplied by  $10^5$ ) and enstrophy  $Q$  in wavenumbers  $k \leq 512$  versus time  $t$ . Note that the initial growth in  $E$  and  $Q$  is approximately exponential.

spectral form

$$\mathcal{E}(k, t) \sim \frac{a_0 k^3}{k^2 + b^2} \tag{2.1}$$

for  $a_0 \approx \text{constant}$  and  $b(t)$  a decreasing function of  $t$  (no faster than  $t^{-1}$  to be consistent with  $\mathcal{E}(k, t) \leq Ck^3 t^2$  for  $k \ll b$ ). This spectral form however is too simple to describe the nearly fixed form of the spectrum for  $k \gg b$ .

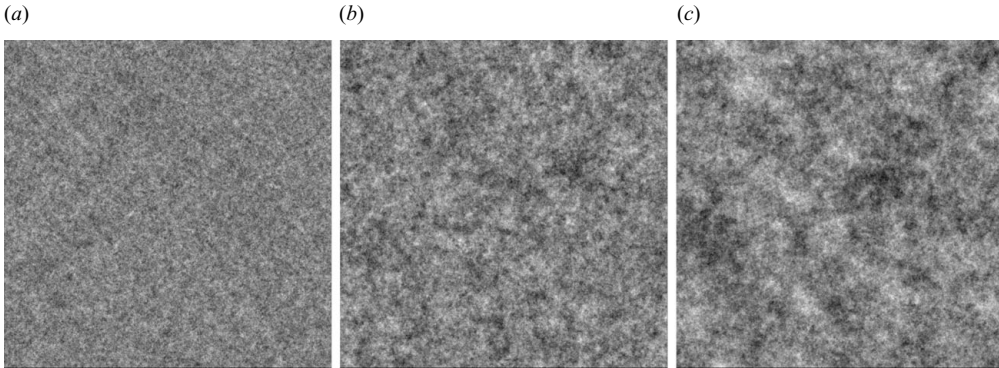


FIGURE 5. Streamfunction  $\psi(x, t)$  at  $t = 200, 500$  and  $2000$  (a–c). A linear greyscale is used from the minimum (black) to maximum (white) values.

That fixed form, we argue, is a consequence of *equipartition*, in which a linear combination of energy  $|\hat{\mathbf{u}}|^2$  and enstrophy  $k^2|\hat{\mathbf{u}}|^2$  spreads itself uniformly among the Fourier modes ( $\hat{\mathbf{u}}(\mathbf{k})$  is the amplitude of the velocity projected on wavevector  $\mathbf{k}$  (Kraichnan 1967). This gives rise to the equipartition spectrum

$$\mathcal{E}_{eq}(k) = \frac{c_1 k}{k^2 + p^2}, \quad (2.2)$$

where the constants  $c_1$  and  $p$  are determined from the total energy  $E = \int \mathcal{E}_{eq} dk$  and enstrophy  $Q = \int k^2 \mathcal{E}_{eq} dk$ , integrated over  $0 \leq k \leq k_{max}$ , where  $k_{max}$  is the maximum wavenumber used in the truncated inviscid dynamical model. Fox & Orszag (1973) illustrate how the spectral shape (controlled by  $p^2$ ) depends on the ratio  $Q/E$ , and discuss the approach to equipartition from non-equilibrium initial conditions. They conducted truncated spectral simulations of inviscid two-dimensional turbulence and confirmed that  $\mathcal{E}(k, t) \rightarrow \mathcal{E}_{eq}(k)$  at late times.

The present point vortex simulation appears to exhibit similar characteristics. It too has truncated dynamics, in the sense that no enstrophy cascade can occur below a certain scale (the individual point vortices are neither created nor destroyed). This appears to be sufficient for the flow to approach equipartition. But the definitive test is how well the spectra in figure 3 match the equipartition spectrum (2.2) for the known values of  $E$  and  $Q$ . Clearly the equilibrium energy spectrum (2.2) does not explain the energy spectrum at large scales where we observe a  $k^3$  range. However since this range is decreasing over time and being invaded by the  $k^1$  spectrum, we may introduce another time-dependent parameter  $b(t)$  and modify (2.2) at low  $k$  to have the form of (2.1), leading to the hybrid spectrum

$$\mathcal{E}(k, t) \sim \frac{ck^3}{(k^2 + b^2)(k^2 + p^2)}. \quad (2.3)$$

We emphasize that this does not have the same sound mathematical basis as (2.2); we have introduced (2.3) simply to model the time-dependent approach to equilibrium. The amplitude  $c(t)$  and the two wavenumbers  $b(t)$  and  $p(t)$  can be determined by fitting to  $E$ ,  $Q$  and the integral  $S = \int k^{-2} \mathcal{E} dk$  which is the mean square streamfunction. The parameter  $b(t)$  measures the departure from the equilibrium spectrum (2.2) and for  $b(t) \rightarrow 0$  we have  $\mathcal{E}(k, t) \rightarrow \mathcal{E}_{eq}(k)$ . Note that  $S$  is not conserved in the exact dynamics, but  $k^{-2} \mathcal{E}$  peaks around the wavenumber  $b$  controlling the transition between large and intermediate scales. Figure 6 shows how well (2.3) matches the actual energy

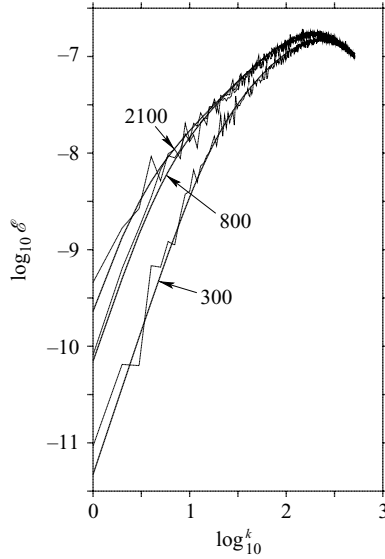


FIGURE 6. Actual energy spectra at  $t = 300, 800$  and  $2100$  (thin lines) compared to hybrid-equipartition spectra (bold lines).

spectra over  $0 \leq k \leq k_{max} = 512$  at early, intermediate and late times in the point vortex simulation. The agreement is excellent across all wavenumbers, and uniformly in time for  $t \geq 300$ . Note that these results are *not* obtained by a least squares curve fit, but merely by equating  $\int k^{-2} \mathcal{E} dk$ ,  $\int \mathcal{E} dk$  and  $\int k^2 \mathcal{E} dk$  for  $\mathcal{E}$  in (2.3) to the known values of  $S$ ,  $E$  and  $Q$  in the point vortex simulation.

The parameters  $b$ ,  $c$  and  $p$  are displayed in figure 7 as a function of time for  $t \geq 300$ . Note that  $c(t)$  and  $p(t)$  rapidly tend to constant values, while the wavenumber  $b(t)$  diminishes like  $t^{-1}$ , consistent with the bound obtained by Tran & Dritschel (2006). For times  $t > 1700$ , the nearly linear increase in  $1/b$  is arrested. At these times, the simulation becomes increasingly affected by the finite box size, preventing further scale growth. But we clearly can see the trend towards the equilibrium spectrum (2.2).

We now consider how equipartition relates to the physical properties of the vortex distribution. Davidson (2007) has shown that a random distribution of vortex dipoles gives rise to a  $k^1$  energy spectrum at scales larger than the dipoles. This suggests that our simulation is dominated by dipoles at scales comparable to the energy-ensrophy scale  $L$  (where the spectrum changes over from  $k^{-1}$  to  $k^1$  around  $k = p$ ). Figure 8 shows that this is indeed the case, each dipole being composed of many point vortices. Note that the scale of the dipoles does not grow appreciably over time, but remains of order  $L$ . Moreover, the dipoles are space filling, and an examination of their time evolution shows that they are short lived (with life times comparable to the ensrophy timescale  $1/Q^{1/2}$ ).

We verify next that this picture is correct, i.e. that at late times the flow is characterized by a sea of dipoles. We first prove, statistically, that a (large) random distribution of dipoles implies that the ensemble mean vorticity  $\langle |\omega| \rangle$  over an area of size  $A$  should scale as  $A^{-3/4}$  (and this result is unique to dipoles). In any sufficiently large area  $A$ , the expected number of dipoles is proportional to  $A$ . Within  $A$ , the dipoles contribute nothing to the mean vorticity, but on the periphery of  $A$ , some halves of dipoles will be in  $A$  and others will not. Hence, there will be a surplus of positive or negative vortices, implying a non-zero mean vorticity  $\langle |\omega| \rangle$ . The mean



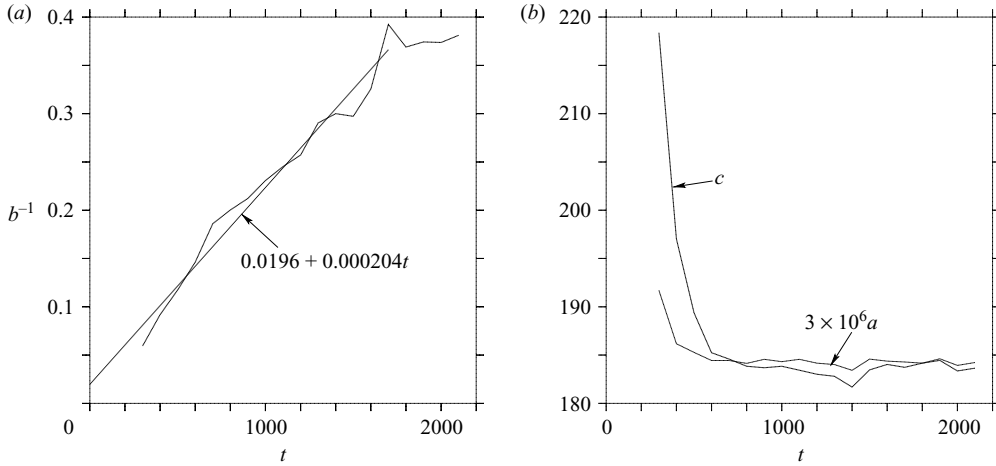


FIGURE 7. Time evolution of (a) the inverse large-scale wavenumber  $b$ , and (b) spectral amplitude  $c$  together with the peak wavenumber  $p$ . The linear fit in (a) was obtained by a least squares analysis over  $300 \leq t \leq 1700$ .

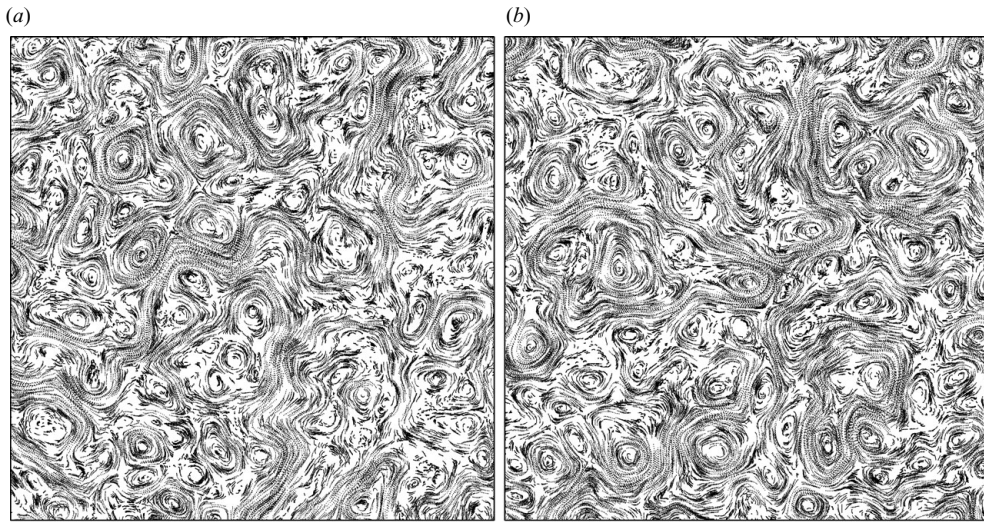


FIGURE 8. Point-vortex trajectories over a single unit of time at (a)  $t = 800$  and (b)  $t = 2000$ . Only a thousandth ( $1/32^2$ ) of the domain is shown. The energy-entrophy scale  $L$  in each case is shown beneath each plot. Note that the characteristic large scale  $2\pi/b \sim 100L$  and is growing nearly linearly in time.

number of randomly distributed surplus vortices scales as the square-root of the number of dipoles on the periphery of  $A$ , since the orientation of the dipoles is uniformly distributed (we thus have Gaussian statistics). But the number of dipoles on the periphery is proportional to the perimeter of  $A$ , which is itself proportional to  $A^{1/2}$ . Hence, the mean number of surplus vortices scales like the square-root of the perimeter, or  $A^{1/4}$ . This divided by the area  $A$  is proportional to the mean vorticity over  $A$ , and therefore  $\langle |\omega| \rangle \propto A^{-3/4}$ . Figure 9 shows just how good this prediction is, over a very wide range of areas  $A$  extending from the grid scale to the domain scale.

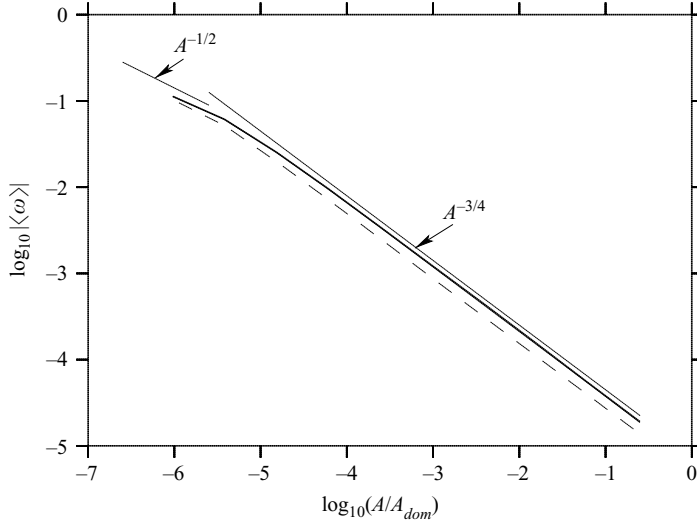


FIGURE 9. Ensemble mean vorticity  $\langle |\omega| \rangle$  versus the sampling area  $A$  in the point vortex simulation at times  $t = 200$  (short-dashed line) and  $600$  (bold). We note that at time  $t = 2000$  the curve is indistinguishable from that at  $t = 600$ . Lines proportional to  $A^{-3/4}$  and  $A^{-1/2}$  are shown for reference. Note that  $L^2/A_{dom} \approx 10^{-5}$  at the latter two times.

Note that a random distribution of vortex monopoles, by similar arguments, would give  $\langle |\omega| \rangle \propto A^{-1/2}$ . A reduction in slope toward  $-1/2$  is just visible in figure 9 at scales smaller than the energy-entropy scale  $L$ . As can be seen from figure 8, these scales are below the scale of the dipoles and are characterized by individual monopoles (the point vortices themselves).

### 3. Late time evolution at all scales

The main limitation of the point vortex model just described is that the individual vortices cannot merge and exhibit an enstrophy cascade ( $p$  is constant in (2.2)). This cascade transfers coherent enstrophy contained within the vortices to filaments, and additionally results in a slow  $t^{1/6}$  growth of large-scale vortices (Dritschel *et al.* 2008). The observed tendency toward equipartition exhibited by the point vortices, however, is a direct result of their stationary population characteristics. Nevertheless, we argue that evolving two-dimensional turbulence will form an equipartition spectrum at large scales, precisely because the evolution is so slow and becomes ever slower in time. Eventually, there is time for equipartition to become established at all but the very largest scales, which must remain bounded by a steeper  $k^3$  spectrum (Tran & Dritschel 2006).

To analyze the numerical results at the large scales we propose here a simple spectral form incorporating three basic elements:

- (a) large-scale equipartition over a range  $k \lesssim m(t)$ ,
- (b) a self-similar vortex population over a range  $m(t) \lesssim k \lesssim f(t)$  and
- (c) a filamentary cascade over a range  $f(t) \lesssim k \lesssim d(t)$ .

A spectral form with these properties is

$$\mathcal{E}(k, t) = \frac{ck(1 + k^2/f^2)}{(k^2 + m^2)^3}. \quad (3.1)$$

We stress that this spectrum is chosen simply to deduce the temporal scaling of the spectral transition wavenumbers. It is not a mathematical model like the equipartition spectrum (2.2) proposed by Fox & Orszag (1973). Here  $m(t)$  is a wavenumber associated with the maximum vortex size ( $m$  can be defined by the coherent energy-*enstrophy* centroid,  $m \approx \sqrt{Q_{coh}/E_{coh}}$ , obtained by integrating the spectrum over the vortex wavenumbers  $m(t) \lesssim k \lesssim f(t)$ ). The wavenumber  $f(t)$  marks the transition scale from vortices to filaments, and  $d(t)$  is the leading edge of the ‘*enstrophy front*’, assumed to be increasing exponentially (see below). The final coefficient  $c(t)$  is proportional to the vortex density (Dritschel *et al.* 2008). Notice that for simplicity we ignore the steep  $k^3$  range at  $k \ll m$ ; this range contributes negligibly to both the energy and the *enstrophy*. Moreover, we do not incorporate the  $k^{-1}$  range of the equipartition spectrum (2.2). This is because the transition from  $k^1$  to  $k^{-1}$  in (2.2) occurs at the energy-*enstrophy* centroid  $p \approx \sqrt{Q/E}$ , which is much larger than its coherent counterpart  $m \approx \sqrt{Q_{coh}/E_{coh}}$ , since  $Q_{coh} \ll Q$  at late times (while  $E_{coh} \approx E$ ).

At sufficiently late times (i.e. many eddy turnaround times based on r.m.s. vorticity), vortex self-similarity predicts  $c(t) \sim t^{-2/3}$  and  $m(t) \sim t^{-1/6}$  (Dritschel *et al.* 2008). However, the ‘*filament transition*’ wavenumber  $f(t)$  is not predicted. Instead here we determine  $f(t)$  from conservation of energy  $E$  and *enstrophy*  $Q$ , together with an assumption on the growth of the ‘*enstrophy front*’ at  $k=d(t)$ . We argue that the thinnest filaments, at the scale  $L_d \propto d^{-1}$ , are essentially passive and thus likely thin exponentially fast, i.e.  $d(t) \sim e^{\gamma t}$  where  $\gamma$  is the mean strain rate associated with larger scales. It is conceivable that  $\gamma$  scales with the r.m.s. vorticity contained within the larger scales, but it seems more plausible that  $\gamma$  scales with the characteristic vorticity magnitude  $\omega_v$  within the vortices, which efficiently capture and twist filamentary debris as they criss-cross space.  $\omega_v$  varies little across the vortex population (Dritschel *et al.* 2008) and is time invariant. The r.m.s. vorticity on the other hand decreases like  $t^{-1/6}$  due to the decreasing area fraction covered by the vortices (Dritschel *et al.* 2008). Since there is little practical difference, we choose the simpler assumption that  $\gamma$  is constant.

This assumption is well supported by simulation results for Navier–Stokes turbulence (Dritschel, Tran & Scott 2007), where it was shown that the palinstrophy  $P$  (or mean square vorticity gradient) reaches a maximum at a time  $t = t_p \approx c_0 + c_1 \ln Re$  where  $Re$  is the Reynolds number. Thereafter,  $P$  decreases by viscous dissipation. But the time  $t_p$  measures the time it takes the *enstrophy front* to reach the scale of viscous dissipation  $\ell_{diss}$ . But  $Re \propto \ell_{diss}^{-2}$ , and hence  $\ell_{diss} \sim e^{-\gamma t_p}$  for some constant  $\gamma$ . Identifying  $\ell_{diss}$  with  $1/d$  in the inviscid context, and  $t_p$  with  $t$ , we arrive again at  $d(t) \sim e^{\gamma t}$ .

We now determine the scaling of the filament transition wavenumber  $f(t)$ . Without loss of generality, we are free to non-dimensionalize length and time by taking  $E = Q = 1/2$ . Using then (3.1), elementary integration yields

$$\frac{4}{c} \int_0^d \mathcal{E}(k, t) dk = \frac{2}{c} = \frac{1}{m^4} + \frac{1}{f^2 m^2} + O\left(\frac{1}{f^2 d^2}\right), \quad (3.2)$$

$$\frac{4}{c} \int_0^d k^2 \mathcal{E}(k, t) dk = \frac{2}{c} = \frac{1}{m^2} + \frac{4 \log(d/m) - 3}{f^2} + O\left(\frac{1}{d^2}\right). \quad (3.3)$$

At late times  $t \gg 1$ , the wavenumbers become increasingly well separated,  $m \ll f \ll d$ , and moreover  $\log(d/m) \sim t \gg 1$ . Retaining therefore only the dominant terms, we have  $c \approx 2m^4$  from energy conservation (which is consistent with  $c \sim t^{-2/3}$  and

$m \sim t^{-1/6}$  found in Dritschel *et al.* 2008) and

$$\frac{1}{m^4} \approx \frac{1}{m^2} + \frac{4 \log(d/m)}{f^2} \quad (3.4)$$

from enstrophy conservation, which implies

$$f \approx 2m^2 \frac{\sqrt{\log(d/m)}}{\sqrt{1-m^2}}. \quad (3.5)$$

At late times,  $m \ll 1$ . Now we use our assumption that the enstrophy front increases exponentially  $d(t) \sim e^{\nu t}$  to obtain the following scaling for the filament transition wavenumber:

$$f \sim t^{1/6}. \quad (3.6)$$

*A posteriori*, this justifies  $m \ll f \ll d$ .

This simple model predicts energy growth  $\mathcal{E}(k, t) \propto t^{1/3} k^1$  in the equipartition range at large scales  $k \ll t^{-1/6}$ , energy decay  $\mathcal{E}(k, t) \propto t^{-2/3} k^{-5}$  over the vortex population at intermediate scales  $t^{-1/6} \ll k \ll t^{1/6}$ , and also energy decay  $\mathcal{E}(k, t) \propto t^{-1} k^{-3}$  over the filamentary range at small scales  $k \gg t^{1/6}$ . The  $k^{-3}$  spectrum is formally the same as that obtained by Batchelor (1969), but in our model this spectrum applies only at high wavenumbers where filaments dominate. Moreover, this spectral tail decays more slowly than predicted by Batchelor. The  $t^{-1}$  decay is due to the exponential stretching of filaments assumed in our model. The spectral tail contains negligible energy and nearly all of the enstrophy.

The spectral evolution for this idealized model is illustrated in figure 10, using  $m = t^{-1/6}$ ,  $d = e^t$ , along with (3.2) for  $c$  and (3.5) for  $f$ . The most striking feature of this evolution is just how slow it is — there is only a small change from  $t = 10$  to  $t = 1000$ . Notice also that the enstrophy at a fixed wavenumber to the left of the peak *increases* for a while before eventually decaying (after the peak sweeps past); nevertheless most of the enstrophy quickly ends up in the rapidly expanding tail between  $k = f$  and  $k = d$ .

#### 4. Comparison with numerical simulations

Support for this simple model is presented next. We carried out 20 high-resolution numerical simulations in a  $2\pi$  doubly periodic domain using the contour-advective semi-Lagrangian (CASL) algorithm (Dritschel & Ambaum 1997; Fontane & Dritschel *in press*). The CASL algorithm is an efficient hybrid contour dynamics/spectral method capable of modelling a wide range of spatial scales with much less numerical dissipation, and much more accurately, than commonly-used algorithms such as pseudo-spectral (Dritschel & Scott 2009). The substantially weaker dissipation in CASL simulations is the result of being able to retain enstrophy to much finer scales (Dritschel & Scott 2009, figures 1–3). Notably, CASL simulations exhibit the same *form* of enstrophy dissipation as in the Navier–Stokes equations, but at a much higher Reynolds number than can be presently achieved with other numerical methods (Dritschel & Scott 2009, figure 4). The simulations reported here would have required approximately  $10^8$  more computational effort if one used the pseudo-spectral method (Dritschel & Scott 2009).

We started each simulation with the energy spectrum  $\mathcal{E}(k, 0) = \alpha k^3 \exp(-2k^2/k_0^2)$ , with  $k_0 = 32$  and  $\alpha$  chosen so that  $E = 1/2$ . Then  $Q(0) = k_0^2/2$ . The maximum wavenumber used to represent the velocity field is  $k_{\max} = 256$  (the vorticity is

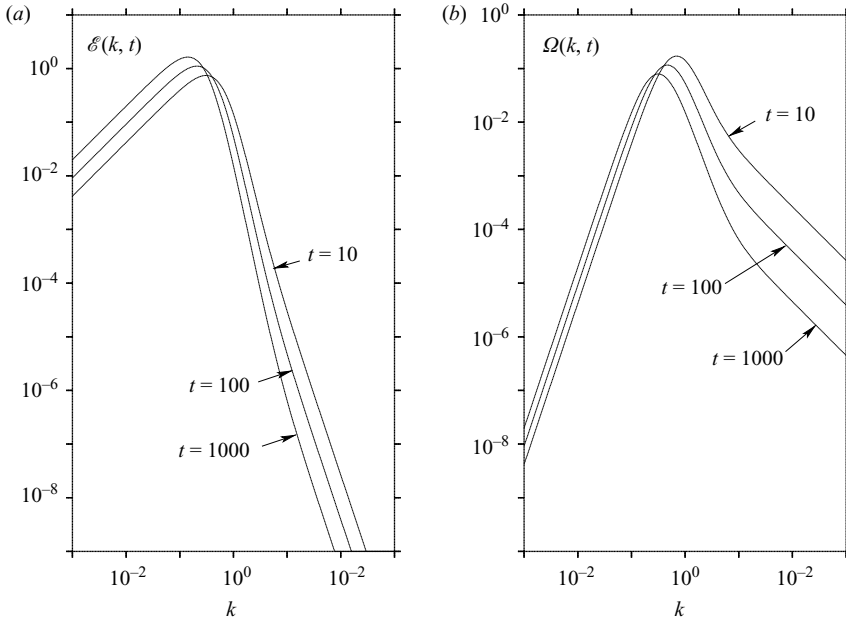


FIGURE 10. Model energy  $\mathcal{E}$  and enstrophy  $\Omega$  spectra (a, b) for the non-dimensional times  $t = 10, 100$  and  $1000$  as labelled. Here, the total energy and enstrophy are both equal to  $1/2$ . Only the range  $10^{-3} \leq k \leq 10^3$  is shown. Logarithmic scales are used.

represented at 8 times higher resolution). Each simulation differed only in a random number seed determining the phases of the Fourier coefficients.

The flow evolution was computed for 160 ‘eddy rotation periods’  $T_{eddy} \equiv 4\pi/\omega_{rms}(0)$ , where  $\omega_{rms}(0) = \sqrt{2Q(0)} = k_0$  is the initial r.m.s. vorticity (the peak vorticity is 4 to 5 times larger). Below, time  $t$  is in units of  $T_{eddy}$ .

This ensemble of simulations was used previously in Dritschel *et al.* (2008) to corroborate our self-similar evolution model of the vortex population. In particular, the numerical results strongly support the development of a universal vortex number density  $n(A, t) \propto t^{-2/3} A^{-1}$  (corresponding to the energy spectrum  $\mathcal{E}(k, t) \propto t^{-2/3} k^{-5}$  over the range of scales containing the vortex population), and a decay of vortex enstrophy and vortex area fraction proportional to  $t^{-1/3}$  over the last 90% of the evolution.

Two snapshots of the vorticity field from one simulation are shown in figure 11. Note the prevalence of filamentary structures at early times and of vortices at later times. The flow is dominated by vortices at all but the earliest times. Figure 12 shows the enstrophy spectrum at early, intermediate and late times. Each spectrum is multiplied by  $t^{2/3}$  so that, in theory, the intermediate ‘vortex wavenumber range’ remains steady. This appears to work well. At low wavenumbers, we observe a  $k^3$  spectrum (which eventually saturates when energy reaches the domain scale), while at small scales we see a slowly retreating  $k^{-1}$  range. The apparently slow decay of the  $k^{-1}$  range of the enstrophy spectrum at large wavenumbers when compared to figure 10 is due to the  $t^{2/3}$  scaling we have applied.

We now quantify this spectral evolution, and compare it to the ideal evolution proposed in §3. To this end, we computed the total ‘resolved’ energy, enstrophy and palinstrophy ( $E_r$ ,  $Q_r$  and  $P_r$ ) over the wavenumbers  $0 < k \leq k_r$  (with  $k_r = 512$  or  $2048$

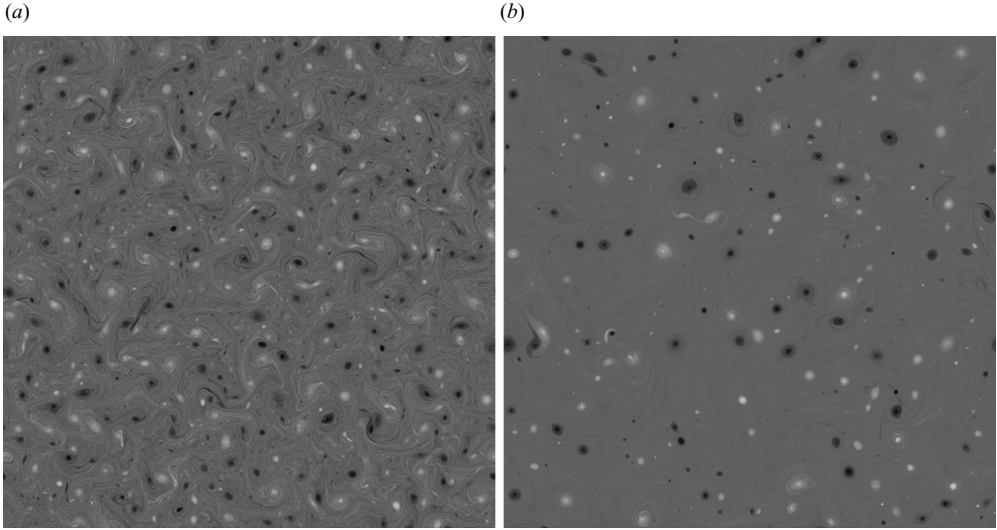


FIGURE 11. Vorticity  $\omega(\mathbf{x}, t)$  at  $t = 6$  (a) and  $t = 24$  (b) in one representative simulation. A linear greyscale is used from the minimum (black) to maximum (white) values.

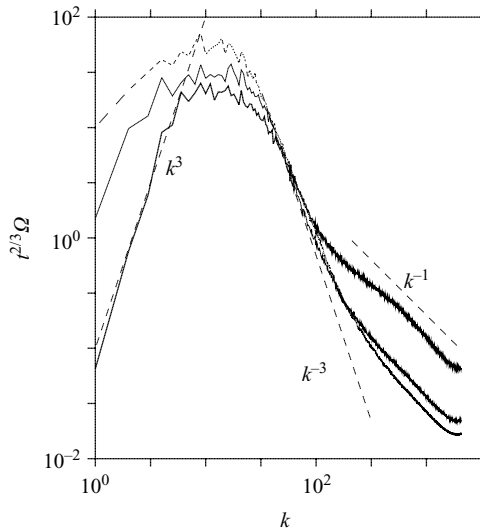


FIGURE 12. Ensemble-averaged scaled enstrophy spectra  $t^{2/3}\Omega(k, t)$  at  $t = 10$  (bold solid line), 40 (thin solid line) and 160 (dashed line). The temporal scaling is intended to collapse the spectra over the range of scales occupied by vortices,  $m \lesssim k \lesssim f$ . Various slopes are indicated.

to check sensitivity). Here, the palinstrophy is given by  $\int_0^{k_r} k^4 \mathcal{E} dk$ , and is equal to the mean square vorticity gradient (divided by 2).  $P_r$  is not conserved in the inviscid limit, but it is used here to help determine the spectral parameters  $c$ ,  $m$  and  $f$  in the idealized spectrum (3.1), for which

$$E_r = \frac{c}{4m^4} + \frac{c}{4f^2m^2}, \tag{4.1}$$

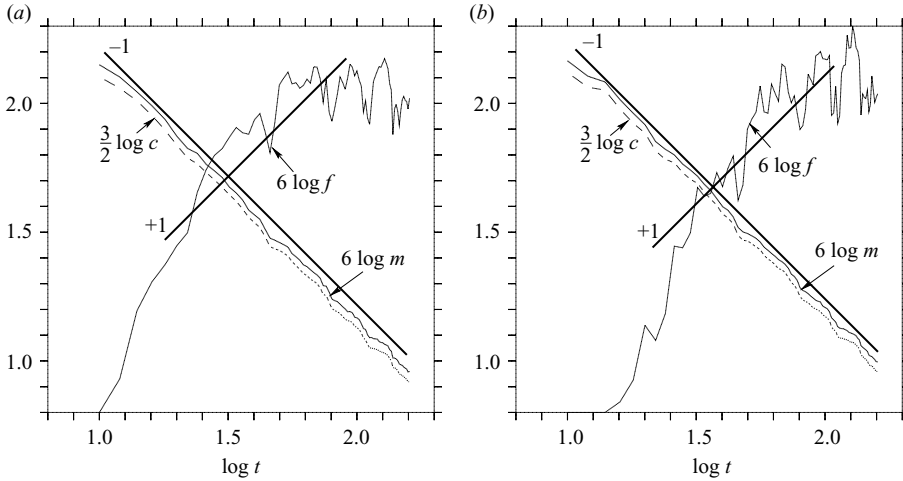


FIGURE 13. Ensemble-averaged spectral parameters  $m(t)$  (bold),  $f(t)$  (thin) and  $c(t)$  (dashed) for two truncation wavenumbers  $k_r = 512$  (a) and  $k_r = 2048$  (b). Note the logarithmic scales. The units on the abscissa are arbitrary (the unscaled parameters are shown in figure 14). Reference slopes of  $\pm 1$  are shown by the thick bold lines.

$$Q_r = \frac{c}{4m^2} + \frac{c}{f^2} \left[ \log(k_r/m) - \frac{3}{4} \right], \quad (4.2)$$

$$P_r = \frac{ck_r^2}{2f^2} \quad (4.3)$$

approximately (for  $k_r \gg f$ ).

The spectral parameters were determined from each simulation from early times  $t = 10$  to the final time  $t = 160$ . They were then ensemble averaged at each time. The resulting ensemble-averaged values of  $m(t)$ ,  $f(t)$  and  $c(t)$  are shown in figure 13 (log scaled) using the truncation wavenumbers  $k_r = 512$  on the left and  $k_r = 2048$  on the right. Figure 14 shows the corresponding unscaled results for  $k_r = 2048$ , emphasizing the slow evolution of the wavenumbers  $m$  and  $f$ . The ‘vortex wavenumber’  $m$  and the ‘vortex density’  $c$  are both insensitive to the choice of  $k_r$ . Using a least squares fit of the log-scaled data, we obtain  $m \sim t^{-0.1702}$ ,  $c \sim t^{-0.6822}$  for  $k_r = 512$  and  $m \sim t^{-0.1676}$ ,  $c \sim t^{-0.6715}$  for  $k_r = 2048$ . These compare well with the theoretical predictions  $m \sim t^{-1/6}$  and  $c \sim t^{-2/3}$  (Dritschel *et al.* 2008).

The results for  $f$  are much less robust, with  $f \sim t^{0.1188}$  for  $k_r = 512$  and  $f \sim t^{0.2105}$  for  $k_r = 2048$ . We argued for  $f \sim t^{1/6}$  in §3 above. The discrepancy at early times occurs because the spectrum has not yet filled out to  $k_r$ . Note from (4.3),  $f$  is determined only by  $P_r$ ; at late times, numerical inaccuracies make  $P_r$  uncertain, particularly as  $P_r$  is dominated by the rapidly fluctuating high- $k$  end of the spectrum. Despite the uncertainty, the numerical data are not inconsistent with our model prediction.

Finally, a comparison of the numerical and ideal model enstrophy spectra at an intermediate time of  $t = 40$  is presented in Figure 15. Again  $c$ ,  $m$  and  $f$  are not fit but determined from  $E_r$ ,  $Q_r$ , and  $P_r$ . The ideal spectrum is more peaked but captures the spectral transitions around  $k = m$  and  $k = f$ , and closely matches the  $k^{-1}$  tail. Importantly, the spectral parameters are *not* sensitive to the form of the ideal spectrum we have chosen, as has been verified using the ‘stick’ spectrum  $\Omega = cm^{-6}k^3$

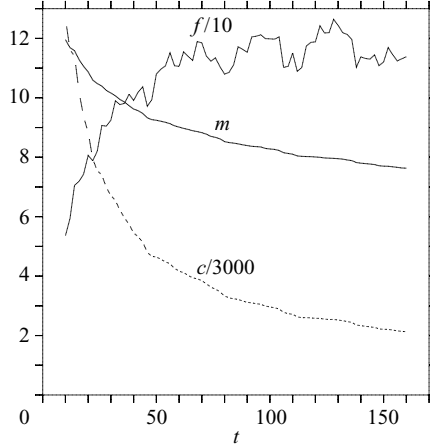


FIGURE 14. Ensemble-averaged spectral parameters  $m(t)$  (bold),  $f(t)$  (thin) and  $c(t)$  (dashed) for  $k_r = 2048$ . Here the scales are linear.

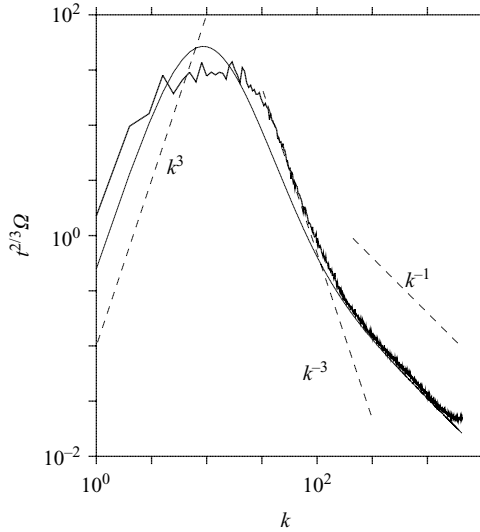


FIGURE 15. Ensemble-averaged scaled enstrophy spectra  $t^{2/3}\Omega(k, t)$  at  $t = 40$  (bold solid line) compared with the ideal scaled spectrum using (3.1). Various slopes are indicated.

joined to  $ck^{-3}$  joined to  $cf^{-2}k^{-1}$ . We do not claim (3.1) is correct everywhere. What appears robust is an energy spectrum containing  $k^1$ ,  $k^{-5}$  and  $k^{-3}$  ranges, with transition wavenumbers evolving according to the time-dependencies discussed. To determine the exact form of the spectrum will require further theoretical insight, such as an improvement of the vortex self-similarity hypothesis near the maximum vortex size.

### 5. Concluding remarks

We have developed a new model for the late-time evolution of inviscid, unforced two-dimensional turbulence. The model builds upon vortex self-similarity over a slowly-expanding intermediate range of scales (Dritschel *et al.* 2008). Here, we propose



that the scales larger than any vortex approach a state of equipartition (Kraichnan 1967; Fox & Orszag 1973), with energy spread uniformly among Fourier modes (except at ultra-large scales, where the energy spectrum is bounded by a constant times  $t^2 k^3$  (see Tran & Dritschel 2006)). Whereas ideal equipartition is a statistically steady state, in our model we argue that the energy spectrum at large scales slowly grows like  $\mathcal{E}(k, t) \propto t^{1/3} k^1$ , and slowly cascades to ever larger scales,  $k \lesssim m(t) \propto t^{-1/6}$ . In particular, the flux of energy to large scales diminishes like  $t^{-5/6}$ . The inverse cascade becomes ever slower.

At small scales, we propose that Batchelor's  $k^{-3}$  spectrum is gradually replaced at its upper end around  $k = f(t) \propto t^{1/6}$  by the steeper spectrum  $\mathcal{E}(k, t) \propto t^{-2/3} k^{-5}$  associated with a self-similar population of vortices (Dritschel *et al.* 2008). The  $k^{-3}$  spectrum, we argue, spreads to high  $k$  exponentially fast, implying that the spectrum decays like  $t^{-1}$  there. This decay is slower than predicted by Batchelor (1969) by simple scale analysis. Furthermore, he did not recognise the possibility that a steeper spectrum would develop and replace the  $k^{-3}$  spectrum at intermediate scales.

We have examined our model's predictions using a large ensemble of high-resolution simulations of two-dimensional turbulence. These simulations strongly support the  $t^{1/6}$  growth of the 'vortex wavenumber'  $m$  (inversely proportional to the size of the largest vortex), and the  $t^{-2/3}$  decay of the 'vortex density'  $c$ . Less secure is our prediction that the 'filament transition wavenumber'  $f$  (where the energy spectrum shallows from  $k^{-5}$  to  $k^{-3}$ ) grows like  $t^{1/6}$ . This wavenumber is sensitive to numerical inaccuracies and to spectral fluctuations at high  $k$ . Nevertheless, our results are not inconsistent with  $f(t) \propto t^{1/6}$ .

Finally, we note that a similar model can be derived for the analogous three-dimensional quasi-geostrophic system applicable to rapidly rotating, strongly stratified flow (Gill 1982). This system is in many ways analogous to the two-dimensional one studied here: it possesses a materially conserved dynamical tracer (potential vorticity), its flow is layer-wise two-dimensional and non-divergent, it has a scalar streamfunction whose Laplacian is the conserved dynamical tracer, and it exhibits a direct enstrophy cascade and an inverse enstrophy cascade (Charney 1971). In the quasi-geostrophic system, equipartition at late times gives rise to a spectrum  $\mathcal{E}(k, t) \propto t^{9/20} k^2$  at large scales, while the emergence of a self-similar population of vortices gives rise to a spectrum  $\mathcal{E}(k, t) \propto t^{-3/4} k^{-6}$  at intermediate scales. Further details and computational support are left for a future study.

Georg A. Gottwald is partly supported by the Australian Research Council grant DP0452147. We wish to thank colleagues and staff at the Isaac Newton Institute (Cambridge) for their feedback and support during the 2008 programme on High Reynolds Number Turbulence.

#### REFERENCES

- BARTELLO, P. & WARN, T. 1996 Self-similarity of decaying two-dimensional turbulence. *J. Fluid Mech.* **326**, 357–372.
- BATCHELOR, G. K. 1969 Computation of the energy spectrum in homogeneous two-dimensional turbulence. *Phys. Fluids* **12**, 233–239.
- BENZI, R., COLELLA, M., BRISCOLINI, M. & SANTANGELO, P. 1992 A simple point vortex model for two-dimensional decaying turbulence. *Phys. Fluids* **4**, 1036.
- BENZI, R., PATARNELLO, S. & SANTANGELO, P. 1988 Self-similar coherent structures in two-dimensional decaying turbulence. *J. Phys. A* **21**, 1221–1237.

- BRACCO, A., MCWILLIAMS, J. C., MURANTE, G., PROVENZALE, A. & WEISS, J. B. 2000 Revisiting freely decaying two-dimensional turbulence at millennial resolution. *Phys. Fluids* **12**, 2931–2941.
- CARNEVALE, G. F., MCWILLIAMS, J. C., POMEAU, Y., WEISS, J. B. & YOUNG, W. R. 1991 Evolution of vortex statistics in two-dimensional turbulence. *Phys. Rev. Lett.* **66**, 2735–2737.
- CHARNEY, J. 1971 Geostrophic turbulence. *J. Atmos. Sci.* **28**, 1087–1095.
- CHASNOV, J. R. 1997 On the decay of two-dimensional homogeneous turbulence. *Phys. Fluids* **9**, 171–180.
- CHRISTIANSEN, J. P. & ZABUSKY, N. J. 1973 Instability, coalescence and fission of finite-area vortex structures. *J. Fluid Mech.* **61**, 219–243.
- CLERCX, H. J. H., MAASSEN, S. R. & VAN HEIJST, G. J. F. 1999 Decaying two-dimensional turbulence in square containers with no-slip or stress-free boundaries. *Phys. Fluids* **11**, 611–626.
- DAVIDSON, P. A. 2004 *Turbulence: An Introduction for Scientists and Engineers*. Oxford University Press.
- DAVIDSON, P. A. 2007 On the large-scale structure of homogeneous, two-dimensional turbulence. *J. Fluid Mech.* **580**, 431–450.
- DRITSCHEL, D. G. & AMBAUM, M. H. P. 1997 A contour-advective semi-Lagrangian algorithm for the simulation of fine-scale conservative fields. *Quart. J. R. Meteorol. Soc.* **123**, 1097–1130.
- DRITSCHEL, D. G. & SCOTT, R. 2009 On the simulation of nearly inviscid two-dimensional turbulence. *J. Comput. Phys.* **228**, 2707–2711.
- DRITSCHEL, D. G., SCOTT, R. K., MACASKILL, C., GOTTWALD, G. A. & TRAN, C. V. 2008 Unifying scaling theory for vortex dynamics in two-dimensional turbulence. *Phys. Rev. Lett.* **101**, 094501.
- DRITSCHEL, D. G., TRAN, C. V. & SCOTT, R. K. 2007 Revisiting Batchelor's theory of two-dimensional turbulence. *J. Fluid Mech.* **591**, 379–391.
- DRITSCHEL, D. G. & ZABUSKY, N. J. 1996 On the nature of vortex interactions and models in unforced nearly-inviscid two-dimensional turbulence. *Phys. Fluids* **8** (5), 1252–1256.
- EYINK, G. L. & SPOHN, H. 1993 Negative-temperature states and large-scale, long-lived vortices in two-dimensional turbulence. *J. Stat. Phys.* **70**, 833–886.
- EYINK, G. L. & SREENIVASAN, K. R. 2006 Onsager and the theory of hydrodynamic turbulence. *Rev. Mod. Phys.* **78**, 87–135.
- FONTANE, J. & DRITSCHEL, D. G. 2009 The HyperCASL algorithm: a new approach to the numerical simulation of geophysical flows. *J. Comput. Phys.* **228** (17), 6411–6425.
- FOX, D. G. & ORSZAG, S. A. 1973 Inviscid dynamics of two-dimensional turbulence. *Phys. Fluids* **16** (2), 169–171.
- GILL, A. E. 1982 *Atmosphere–Ocean Dynamics*. Academic.
- JOYCE, G. & MONTGOMERY, D. 1973 Negative temperature states for the two-dimensional guiding center plasma. *J. Plasma Phys.* **10**, 107–121.
- KRAICHNAN, R. H. 1967 Inertial ranges in two-dimensional turbulence. *Phys. Fluids* **10**, 1417–1423.
- LAVAL, J. P., CHAVANIS, P. H., DUBRULLE, B. & SIRE, C. 2001 Scaling laws and vortex profiles in 2D decaying turbulence. *Phys. Rev. E* **63**, 065301R.
- LESIEUR, M. 2008 *Turbulence in Fluids*, 4th edn. Springer.
- LOWE, A. J. & DAVIDSON, P. A. 2005 The evolution of freely-decaying, isotropic, two-dimensional turbulence. *Eur. J. Mech. B/Fluids* **24**, 314–327.
- MCWILLIAMS, J. C. 1984 The emergence of isolated coherent vortices in turbulent flow. *J. Fluid Mech.* **146**, 21–43.
- MILLER, R. 1990 Statistical mechanics of negative temperature states. *Phys. Rev. Lett.* **65**, 2137–2140.
- MONTGOMERY, D. & JOYCE, G. 1974 Statistical mechanics of negative temperature states. *Phys. Fluids* **17**, 1139–1145.
- ONSAGER, L. 1949 Statistical hydrodynamics. *Nuovo Cimento* **6**, 279–287.
- ORSZAG, S. A. 1970 Analytical theories of turbulence. *J. Fluid Mech.* **41**, 363–386.
- OSSAI, S. & LESIEUR, M. 2001 Large-scale energy and pressure dynamics in decaying 2D incompressible isotropic turbulence. *J. Turbul.* **2**, 172–205.
- ROBERT, R. 1991 A maximum-entropy principle for two-dimensional perfect fluid dynamics. *J. Stat. Phys.* **65**, 531–554.

- ROBERT, R. & SOMMERIA, J. 1991 Statistical equilibrium states for two-dimensional flows *J. Fluid Mech.* **229**, 291–310.
- SIRE, C. & CHAVANIS, P. H. 2000 Numerical renormalization group of vortex aggregation in 2D decaying turbulence: the role of three-body interactions. *Phys. Rev. E* **61**, 6644–6653.
- TABELING, P. 2002 Two-dimensional turbulence: a physicist approach *Phys. Rep.* **362**, 1–62.
- TRAN, C. V. & DRITSCHEL, D. G. 2006 Large-scale dynamics in two-dimensional Euler and surface quasigeostrophic flows. *Phys. Fluids* **18**, 121703.
- WEISS, J. B. & McWILLIAMS, J. C. 1993 Temporal scaling behavior of decaying two-dimensional turbulence. *Phys. Fluids* **5**, 608–621.